Cancer cell detection and invasion depth estimation in brightfield images

Pedro Quelhas[1]
quelhas@fe.up.pt
Monica Marcuzzo[1]

Ana Maria Mendonça[1,2]
amendon@fe.up.pt
Maria José Oliveira[1]
mariajo@ineb.up.pt
Aurélio Campilho[1,2]
campilho@fe.up.pt/

[1] INEB - Instituto de Engenharia Biomédica, Porto, Portugal

[2] Universidade do Porto, Faculdade de Engenharia, Departamento de Engenharia Electrotécnica e Computadores

Abstract

The study of cancer cell invasion under the effect of different conditions is fundamental for the understanding of the invasion mechanism and to test possible therapies for its regulation. In this study, to simulate cancer cell invasion across tissue basement membrane, biologists established *in vitro* invasion assays with cancer cells invading extracellular matrix components. However, analysis of the assay is manual, being time-consuming and error-prone, which motivates an objective and automated analysis tool.

With the objective of automating the analysis of cell invasion assays we present a new methodology to detect cells in 3D matrix cell assays and correctly estimate their invasion, measured by the depth of the penetration in the gel. Detection is based on the sliding band filter, by evaluating the gradient convergence and not intensity. As such it can detect low contrast cells which otherwise would be lost. For cell depth estimation we present a new tool based on the analysis of cell detections from multiple brightfield images taken at different depths of focus, using a new focus estimation approach based on the convergence gradient's magnitude. The final cell detection's precision and recall are of 0.896 and 0.910 respectively, and the average error in the cell's position estimate is of $0.41\mu m$, $0.37\mu m$ and $3.7\mu m$ in the x, y and z directions, respectively.

1 Introduction

Invasion, an important step in the development of cancer, consists on the extravasation of cells from the tissue of origin into neighbor tissues. While invading, cancer cells establish a continuous molecular crosstalk with host elements of the surrounding microenvironment. In the case of gastric microenvironment, such elements consist of extracellular matrix components, bacteria and host cells, such as fibroblasts, myofibroblasts, endothelial cells, and macrophages. The absence of good models to study the interactions between invasive cancer cells and the other elements of the tumor microenvironment, led to the construction of

BMVC 2009 doi:10.5244/C.23.68

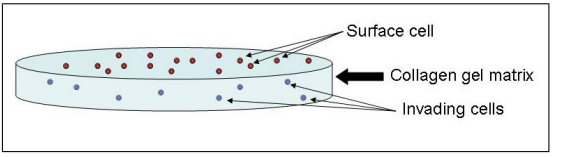

Figure 1: Scheme of the cell invasion assay: a dish well is made to contain a certain amount of gel upon which cells are deposited (red surface cells). With the passing of time cancer cells invade the gel matrix (blue invading cells).

innovative 3D invasion assay [2]. However, the task of evaluating the results of such assays is performed manually by microscopic observation, which is time-consuming, fatiguing, and prone to human errors, requiring frequent repetitions towards validation [2]. These limitations constitute a clear motivation for integrating automation in the analysis of such assays.

Most 3D analysis of cells is based on confocal microscopy which has the capacity to image a single focal plane with little or no interference from out of focus objects [1, 4]. However, researchers use brightfield microscopy which is much simpler and allow for the observation of cells at different depths, which increases the difficulty of cell detection and cell depth estimation. Cell depth is in this case characterized by the best focal plane and is based on the variation of depth of focus.

We present a tool to evaluate 3D cell invasion based on the analysis of multiple brightfield images taken at different depths of focus, using a new estimation approach. Cell depth is in this case characterized by the best focal plane and is based on the variation of depth of focus towards the surface focus.

Automated cell analysis in microscopic images has been explored by many applications. However, most automated cell analysis approaches are based on segmentation [3, 7]. While often used, segmentation for cell detection is semi-automated at best and requires frequent parameter readjustments due to image variability. The most prominent problem with segmentation is its inability to deal with cell clusters, which are detected as one entity. To obtain a successful detection even at low contrast we investigate the use of a particular convergence filter, the Sliding Band Filter (SBF) [8], for cell detection in brightfield microscopy images. SBF is based on image gradient convergence and not intensity. As such, it can detect low contrast cells which otherwise would be lost in the background noise.

The main problem in the analysis of cancer cell invasion assays is that due to the brightfield imaging and the cell's transparency, cells appear at several focal planes giving rise to multiple detections. To solve the multiple detection problem we propose the use of 3D location information by stacking multiple detections and filtering out false detections. From these 3D stacks of cell detection we present a focus measure to estimate the degree of focus of each detection, determining in this way the location of each cell in 3D. This is the final desired result and provides all necessary information to analyse the invasion assay.

This paper is organized as follows: Section 2 describes the biology experiments and data, Section 3 describes our cell detection approach and our cell depth estimation approach. In section 4 we present the results. Finally, conclusion is presented in Section 5.

2 Biological Experimental Setup and Data Collection

In their general formulation cancer cell invasion assays consist of gels of extracellular matrix components (collagen type I or Matrigel, for instance), on top of which isolated cancer

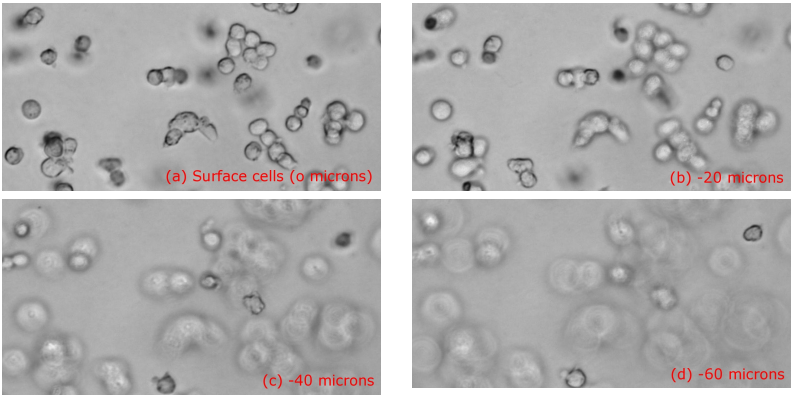

Figure 2: Images from the 3D focus stack from a cancer cell invasion assay (croped to fit figure). Images obtained focused on the surface of the gel where most cells are, at $-20\mu m$ where some invading cells can already be seen, at $-40\mu m$ and $-60\mu m$ where only invasive cells can be seen in focus.

cells, treated or not with specific drugs, are added (Figure 1).Alternatively, the extracellular matrix might be intermixed or not with other host cells (such as fibroblasts, endothelial cells or macrophages. After 24 hours of incubation at 37° C and 5% CO_2 atmosphere, the system is visualized using an inverted Zeiss microscope.The experiments used to validate our methodology were prepared by adding naturally invasive or non-invasive cancer cells, in the absence of any additional treatment, to the top of collagen type I gels without cancer cells intermixed. In the case of the experiments used to validate our methodology collagen gel was used and no macrophages or fibroblasts were introduced into the culture.

To obtain the image data which will enable us to estimate cell invasion, a stack of images is collected varying the depth of focus. The images are collected from a depth above the surface until past the depth of the most invasive of all cells within the field of view, with focus being varied in $5\mu m$ steps. The joint focal length and camera CCD resolution give a spatial scale of $0.256\mu m$ per pixel, each image size being 1388×1040 pixels. Examples of the collected images can be seen in Figure 2.

2.1 In focus definition

Cells in brightfield images are viewed as 3D transparent objects and as such it is required to define which is the in-focus plane for a specific cell. This is a subjective qualification as the cells are partially in focus in several planes, and many decisions could be made. In fact most definitions, as long as precise and coherent, can lead to valid invasion evaluation results since the resulting depth estimation would only be translated. However, the equatorial plane of the cell (assuming cells are spherical) is used in this paper as it allows for the best cell membrane definition for cell width estimation and easier separation of overlapping cells. In Figure 3 several in focus cells are marked, including a touching/overlapping cell group. It can be seen that cells are visible in multiple images, but they were marked in the image where imaging of cell walls is sharper, leading to a more precise cell detection.

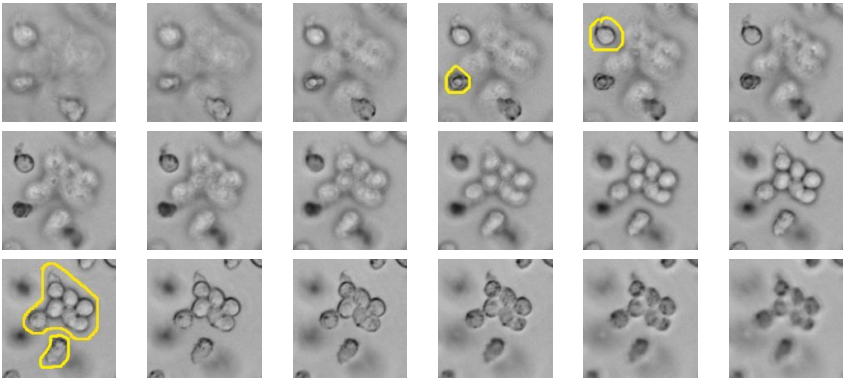

Figure 3: Detail of focus images through varying focus lengths (from $-60\mu m$ (top left) to $+25\mu m$ (bottom right) relative to the surface; in-focus cells are marked at the respective focal plane where the cell membrane is sharper.

3 Methodology

To evaluate the cancer cell invasion in 3D collagen matrix assays we need first to detect all possible cells at all focus depths, then decide which detections correspond to valid cell locations and finally evaluate the most likely depth for each detected cell. As such our methodology can be divided into three steps:

- Cell detection in each image. As each image contains in focus and out of focus cells, the amount of detected cells be larger than the total number of cells in the 3D volume.
- After 2D detection we search for cell detection, at adjacent planes, which are close to each other, associating them in a stack, each representing a possible cell at a determined (x,y) location. However, the z or depth for each cell is still unknown.
- Finally, for each detection stack, estimation of the most likely image plane for the cell's location. This enables the determination the 3D position for each cell.

The following sections give details on each of the steps in our methodology.

3.1 2D Cell Detection

For the task of cell detection we base our decision on image enhancement through filtering, where locations which correspond to cell will have strong filter response. Subsequently, cells are associated with the locations of filter maxima response.

Most cell detection approaches are based on image segmentation. These approaches assume that cells are mostly isolated with few agglomerated cases that must be solved [3, 7]. However, in our case, cell's appear often in groups and, as they are in a 3D structure, can appear superimposed and with different intensities (different focus level). The difficulty of segmentation also increases due to the fact that the images in this case are obtained by brightfield microscopy.

Our approach to cell detection is based on finding the approximated round shape characteristic of cells. To perform such detection we use a convergence index filter [5]. Con-

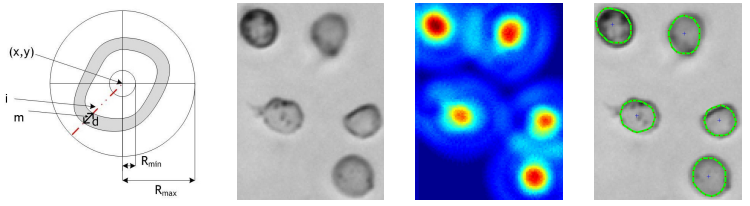

(a) (b) (c) (d)

Figure 4: SBF filter schematics (a), and examples of cell detection using the SBF filter: (b) brightfield image containing in-focus, out-of-focus and grouped cells, (c) filter response for image (b), (d) final detection of cells in the image.

vergence Index (CI) filters are based on the maximization of the convergence index at each image point of spatial coordinates (x,y), defined by:

$$C(x,y) = \frac{1}{M} \sum_{(k,l)\in R} \cos\theta(k,l), \tag{1}$$

where M is the number of points in the filter support region R, θ is the angle between the gradient vector calculated for point (k,l) and the direction of the line that connects points (x,y) and (k,l).

The main difference between distinct CI filters is the definition of the support region R, which is formed by radial lines that emerge from the point where the filter response is being calculated, as shown in Figure 4(a). There are several CI filters: coin filter (CF) [5], iris filter (IF) [5], adaptive ring filter (ARF) [5, 10] and the recently proposed sliding band filter (SBF) [8]. The CF uses a circle with variable radius as support region, the IF maximizes the convergence index by adapting the radius value on each direction and the ARF uses a ring shaped region with fixed width and varying radius. Finally, the SBF combines the basic ideas of IF and ARF by defining a support region formed by a band of fixed width, whose position is changed in each direction to allow the maximization of the convergence index at each point. The set of band positions that maximizes the convergence index at each point will be called as band support points. The more generic formulation of the SBF gives a wider detection range of shapes in comparison with other convergence filters. This is desirable for our application due to possible variations in the shapes that the cells can exhibit. SBF is defined by:

$$SBF(x,y) = \frac{1}{N} \sum_{i=1}^{N} \left(\max_{R_{min}\le n\le R_{max}} \left(\frac{1}{d} \sum_{m=n-d/2}^{n+d/2} \cos(\theta(i,m)) \right) \right), \tag{2}$$

where N is the number of support region lines that irradiate from (x,y), d is the band width, n is the position of the band in a line that varies from R_{min} to R_{max}, and $\theta(i,m)$ is the angle between the image gradient vector direction at location m and the direction that is currently being analyzed i (see Figure 4(a) for filter design schematics).

However, the SBF detects only convergence or divergence. In the case of cell image in brightfield microscope the cytoplasm is not visible, only the cell membrane is visible. This membrane is a location of both convergence and divergence. By ignoring the sign of the convergence factor $\cos(\theta(i,m))$ in the SBF filter we can modify the filter to best fit the

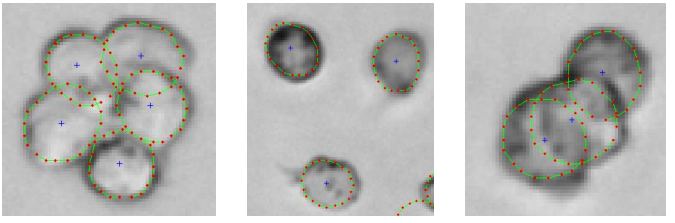

(a) (b) (c)

Figure 5: Examples for MSBF cell detections (a) and (b). Detail of cell detection in the occurrence of severe overlap of cells (c). Red points represent the band support points (point of stronger convergence). The cell membrane is considered the line connecting all band support points (green line).

location we aim at detecting. The Modified Sliding Band Filter (MSBF) is given by:

$$MSBF(x,y) = \frac{1}{N}\sum_{i=1}^{N}\left(\max_{R_{min}\leq n\leq R_{max}}\left(\frac{1}{d}\sum_{m=n-d/2}^{n+d/2}\|\cos(\theta(i,m))\|\right)\right), \tag{3}$$

After the application of the MSBF filter, cells are associated with the locations of filter maxima response. The maxima are obtained by non-maxima suppression filtering and a minimum distance of R_{min} between maxima is enforced.

After locating the cell's center coordinates, we must estimate their shapes and sizes in order to complete their detection. To do so we investigate, for each filter maximum, what were the positions of the sliding band that contributed to that particular maximum. These are the band support points $SP = \{(x_{SP}(i), y_{SP}(i)), i = 1\ldots N\}$ and are defined as:

$$\begin{aligned} x_{SP}(i) &= x + n_{max}(i)\cos\left(\tfrac{2\pi}{N}(i-1)\right) \\ y_{SP}(i) &= y + n_{max}(i)\sin\left(\tfrac{2\pi}{N}(i-1)\right) \\ n_{max}(i) &= \arg\max_{R_{min}<n<R_{max}}\left(\tfrac{1}{d}\textstyle\sum_{m=n-d/2}^{n+d/2}\cos(\theta(i,m))\right) \end{aligned} \tag{4}$$

where N is the number of support region lines and $n_{max}(i)$ corresponds to the radius of the support point for support region line i.

In fact, the position of the band that maximizes the convergence index response in each direction of the MSBF region of support gives an indication of the cells' border location in that specific direction (Figure 4(d) and 5). The final border for the cell detection is the line connecting the band support points. The final detection result gives the 2D locations of cells in each image. The cell detection result can include in-focus cells, detections of the out-of-focus image of cells from adjacent planes or noise triggered detections.

3.2 Cell Detection Stacking

Given all the cells detected in each individual 2D image plane of the 3D stack of images we must now relate each cell in a 2D plane with all possible corresponding cells. This is performed based on a 2D distance between cells in adjacent planes, with the requirement of reciprocity. For each cell detection d in image I, with coordinates $(x_{(I,d)}, y_{(I,d)})$, the 2D distance to all other cell detections in the adjacent plane is obtained and the closest detection d' for image $I+1$ at location $(x_{(I+1,d')}, y_{(I+1,d')})$ is considered to correspond to the same cell.

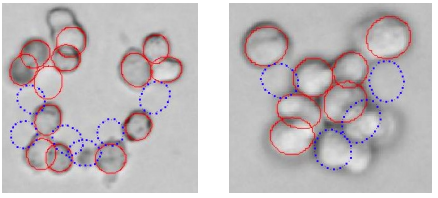

Figure 6: Detections after stacking: blue dotted contours are detected cells which did not get stacked due to non-conformity with stacking requirements. Also visible are some cells which were not detected and have no contour.

Cell detection correspondence is only valid if the 2D distance between d and d' is lower than a threshold and if the closest detection criteria is reciprocal (d must be the closest detection to d' for all possibilities in image I). The final 3D stack is composed of the detection indexes d for each image plane in the stack, or zero in the case where the stack has no detections.

Additionally we also impose continuity of stacks (splitting stacks if there is no correspondence) and impose a minimum number of detections for a stack of cells to be valid. Using these constraints reduces the probability that erroneous detections may be stacked as it is unlikely for noise to be spatially consistent in z. More details on the specific values used for this implementation are presented in the result section.

3.3 Depth Estimation

One of the MSBF filter main properties is that its result is not depending on the magnitude of the image's gradient. This is particularly useful for the specific application of cell detection, allowing the detection even when image contrast is reduced. Moreover, we propose to use this gradient magnitude information to estimate cell depth for the detected cells.

We propose a focus estimator based on the magnitude of the convergence at the band support points. It is a know property from depth from focus methods that an object is more focused if its borders are sharper [6, 9]. As such we define the focus estimation measure as:

$$FE(x,y) = \frac{1}{N}\sum_{i=1}^{N}\left(\frac{1}{d}\sum_{m=n_{max}(i)-d/2}^{n_{max}(i)+d/2} mag(grad(i,m)) * \|\cos(\theta(i,m))\|\right), \tag{5}$$

where $mag(grad(i,m))$ is the gradient magnitude of the image at location m in the i filter's support line and $n_{max}(i)$ is the support point for support region line i.

For a given (x,y) coordinate we can now obtain a focus estimation which has a higher value if those coordinates correspond to an in-focus cell than if they correspond to an out-of-focus cell. In Figure 7 we can observe the value (rounded) of the focus estimator for a cell over several images taken at different focal depths. The progression of the focus estimation value is intuitive and in accordance with the definition of in-focus cell proposed in section 2.

Focus estimator value is also used to validate the cell detection stacks. If a detection stack does not have a minimum value of focus for any cell detection it is assumed that the stack contains detection of a cell that is never in focus (or noise), as such it is removed.

4 Results and Discussion

To evaluate the proposed methodology we use a dataset of 4 independent invasion assays where a total of 84 image planes where collected, every $5\mu m$ in depth. The total sum of cells

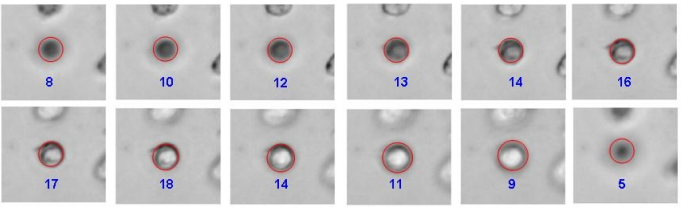

Figure 7: Focus estimator value for a given cell for several focus planes.

in the dataset is of 320. To set the parameters for out methodology an auxiliary (independent) dataset was used with 25 images, containing 70 cells, from an additional invasion assay.

The dataset was annotated, by a researcher under supervision of the project's leading biologist, by selecting the best (x,y,z) coordinate for each cell. This annotation was used to evaluate the presented methodology's performance. The protocol used was based the on distance between annotation and detection, imposing a threshold of 10 pixels and a reciprocal minimal distance between annotation and detection. Cell that obey this criteria are considered to be correctly detected.

4.1 Parameter Settings

Using the auxiliary dataset we set the parameters for cell detection and detection stacking so that results were at the equal error rate between false and miss detections.

For the MSBF filter parameters we chose: $R_{min} = 5$, $R_{max} = 20$, $q = 5$, $N = 32$. These were selected both by visual inspection of the results and by setting the parameters close to those known from the data (empirically some parameters are related to the intrinsic properties of the cells in the images, cell size gives indication of the adequate values for R_{min}, R_{max} and q). However, it was found that cell detection using the MSBF is robust to parameters, with many different parameter setting producing visually similar results. For detection stacking (second step in the methodology) we chose a distance threshold of 10 pixels.

The depth estimation step has no new parameters and uses those set for the MSBF filter. However, for an increase in robustness we impose a minimum of 5 for the focus measure for any final cell detection. This setting was set for the equal error rate in the validation set.

4.2 Cell Detection

We applied the MSBF filter to all images in the test dataset and obtained all detection for each plane, we then stacked and searched for the best candidate for the in-focus plane. Finally, we evaluated the correspondences to the annotation as described before. Table 1 shows the cell detection results. The average precision and recall for the presented methodology is of 0.896 and 0.910 respectively and the average number of false positives and false negatives are of 8.75 and 7.5 respectively. No evaluation of the correctness of detected cells' shape was performed since the annotation does not contain ground truth for the cells' shape These numbers do not change greatly with the distance threshold as the reciprocal requirement for correspondences is stricter than the distance threshold. It was found that the most influential parameter for error regulation is the minimum focus estimate threshold in stack validation.

4.3 Depth Estimation

In addition to evaluate the cell detection in the 3D cell matrix we need to evaluate what are the errors in the positioning in the final cell's coordinates. It is not enough to ensure that

Table 1: Cell detection results:precision, recall and error values for the comparison between detected and annotated cells. Results are presented for each experiment and averaged overall.

	False positives	False negatives	Precision	Recall	number of cells
Dataset1	11	14	0.885	0.859	96
Dataset2	4	6	0.939	0.910	67
Dataset3	12	6	0.876	0.934	91
Dataset4	8	4	0.886	0.939	66
Overall (average)	8.75	7.5	0.896	0.910	80

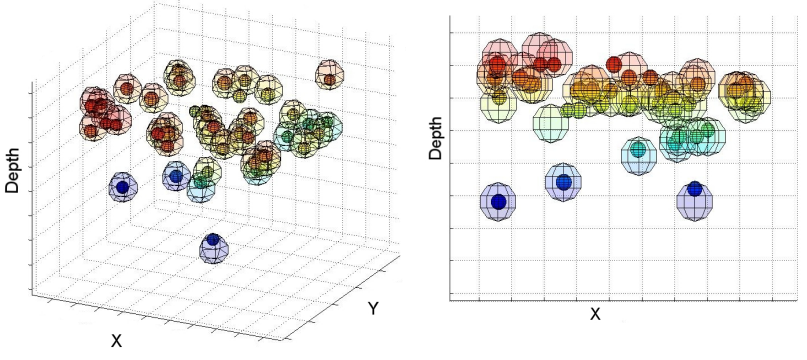

Figure 8: Final 3D detection: smaller spheres with solid colors represent detected cells, larger semi-transparent spheres represent ground truth (all spheres have the same shape and size). Color legend: Blue cells are more invasive, red are more superficial.

the detected cell is within 10 pixels of the annotated cell. It is necessary to measure the real error for each detection. Table 2 shows the average error for the cell's detection (x, y, z) coordinates for each experiment and overall, measured as the Euclidean distance from the cells detections to the corresponding annotation.

5 Conclusion

We evaluated a new focus estimator for cell invasion depth estimation in brightfield images, based on of the Sliding Band Filter for cell detection. This methodology was validated using brightfield microscopy images of cancer cell invasion assays.

The results obtained using a database of 4 experiments, corresponding to 84 images and 320 cells, show a cell detection precision and recall of 0.896 and 0.910 respectively. Additionally we analyzed the magnitude of the cell detection's positional errors and found that in average the x, y and z errors were of $0.41\mu m$, $0.37\mu m$ and $3.7\mu m$ respectively.

Visual inspection showed that most cell detection errors occurred at the gel's surface. This was to be expected since surface cells group and overlap more. This is important as it indicates that invading cell detection is mostly correct and these are the most important the assay analysis.

Overall the results were both numerically and visually promising for the construction of a fully automated cell invasion quantification application (figure 8).

The next steps in the search for an objective invasion assay evaluation are the determination of the surface z location and the computation of the percentage of cells invading. However, determining the surface is both obscured by the noise in depth detection and complicated since cells stack and move the gel matrix causing an undetermined depth variation.

Table 2: Cell's position estimation error: for each experiment the average x, y and z error in the cell's position are presented, as well as the overall position errors (values in μm).

	x average error	y average error	z average error
experiment1	0.44	0.41	4.8
experiment2	0.40	0.32	3.5
experiment3	0.35	0.36	3.2
experiment4	0.45	0.40	3.5
Overall	0.41	0.37	3.7

Acknowledgements

The authors acknowledge the funding of Fundação para a Ciência e Tecnologia.

References

[1] Sarti A, de Solorzano CO, Locket S, and Malladi R. A geometric model for 3-d confocal image analysis. *IEEE Trans. on Biomedical Engineering*, 47:1600–1609, 2000.

[2] Marc E. Bracke, Tom Boterberg, Eric A. Bruyneel, and Marc M. Mareel. Collagen invasion assay. *Methods in Molecular Medicine, Academic Press*, 58:Metastasis Research Protocols:81–87, 1999.

[3] X. Chen, X. Zhou, and S. T. C. Wong. Automated segmentation, classification, and tracking of cancer cell nuclei in time-lapse microscopy. *IEEE Trans. on Biomedical Engineering*, 53(4):762–766, 2006.

[4] A. Dufour, V. Shinin, S. Tajbakhsh, N. Guillen-Aghion, J.-C. Olivo-Marin, and C. Zimmer. Segmenting and tracking fluorescent cells in dynamic 3-d microscopy with coupled active surfaces. *IEEE Transactions on Image Processing*, 14:1396 – 1410, 2005.

[5] H. Kobatake and S. Hashimoto. Convergence index filter for vector fields. *IEEE Trans. on Image Processing*, 8(8), 1999.

[6] James G. McNally, Tatiana Karpova, John Cooper, and Jose Angel Conchello. Three-dimensional imaging by deconvolution microscopy. *Methods*, (3):373–385, November 1999.

[7] Maria Hasse Oliver Schmitt. Morphological multiscale decomposition of connected regions with emphasis on cell clusters. *Computer Vision and Image Understanding*, 113:188–201, 2009.

[8] C. S. Pereira, H. Fernandes, and A. M. Mendonça e A. Campilho. Detection of lung nodule candidates in chest radiographs. *LNCS*, 4478:170–177, 2007.

[9] Favaro Mennucci Soatto, P. Favaro, A. Mennucci, and S. Soatto. Observing shape from defocused images. *International Journal of Computer Vision*, 52:25–43, 1999.

[10] J. Wei, Y. Hagihara, and H. Kobatake. Detection of rounded opacities on chest radiographs using convergence index filter. In *Proceedings of the Int. Conference on Image Analysis and Processing*, pages 757–761, 1999.